International Journal of Applied Electromagnetics and Mechanics 16 (2002) 153–161
IOS Press

Classical and IT based magnetization dynamics modeling

Hisashi Endo[a,*], Yoshifuru Saito[a], Seiji Hayano[a] and Kenzo Miya[b]
[a]*Graduate School of Engineering, HOSEI University, 3-7-2 Kajino, Koganei, Tokyo 184-8584, Japan*
[b]*International Institute of Universum, 8F SB Bldg., 1-4-6 Nezu, Bunkyo, Tokyo 113-0031, Japan*

Abstract. This paper reviews the classical magneitization models for computation use, and also proposes information/intelligence technology (IT, in short) based model for the magnetodynamics in ferromagnetic materials. At first, Fourier model of the hysteretic magnetization is derived. Second, assuming the bar-like domain walls derives a domain-based model. This model is verified by a simple example. Third, a composite model by combining the Preisach with domain-based models is derived, and then, Rayleigh's law is derived. Finally, IT based model for magnetodynamics in ferromagnetic materials is introduced.

1. Introduction

Modeling of the ferromagnetic materials is of paramount importance for modern computational magnetodynamics in order to carry out the practical magnetic device design. Fundamentally, the elements comprising the modern electronic as well as electrical devices are classified into two major categories. One is the active element such as silicon controlled rectifier and Power MOS FET. The other is the passive element such as resistance, capacitance and inductance. Even if the inductors are regarded as one of the linear elements in the undergraduate textbook, practically most of them exhibit a serious non-linearity, e.g., saturation and hysteretic properties.

In the present paper, at first, we derive a phenomenological magnetization model by means of Fourier series. Second, assuming the bar-like domain walls leads to a domain-based model. Third, a composite model by combining the Preisach with domain-based models is derived. Analytical solution of this composite model leads to famous Lord Rayleigh's law. Finally, we propose the IT based magnetization model utilizing digital computers and its network under the Internet infrastructure. Therefore, this IT based model is derived the digital images. Practically this IT based model is applied to SEM images of grain oriented silicon steel sheet. We recover the magnetization characteristics at the normal, lancet and strained magnetic domains on the SEM image. Thus, this paper suggests an implementation methodology of computer-aided magnetic device design fully taking into account the magnetization characteristics in ferromagnetic materials.

*Corresponding author: Tel.: +81 42 387 6200; Fax: +81 42 387 6200; E-mail: endo@ysaitoh.k.hosei.ac.jp.

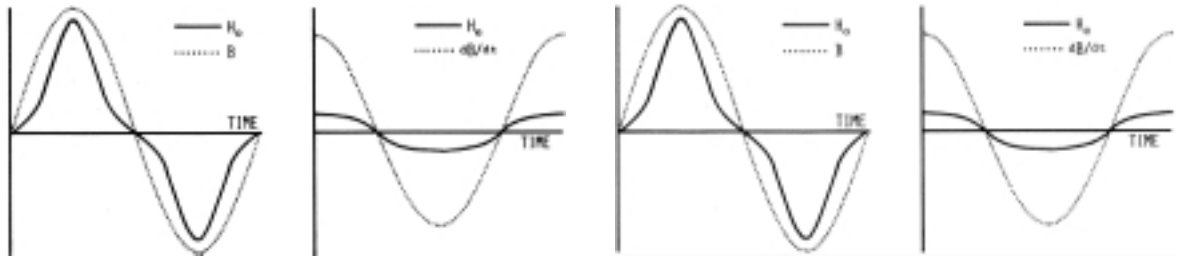

(a) (b) (c) (d)

Fig. 1. Typical hysteresis loop and time in phase components.

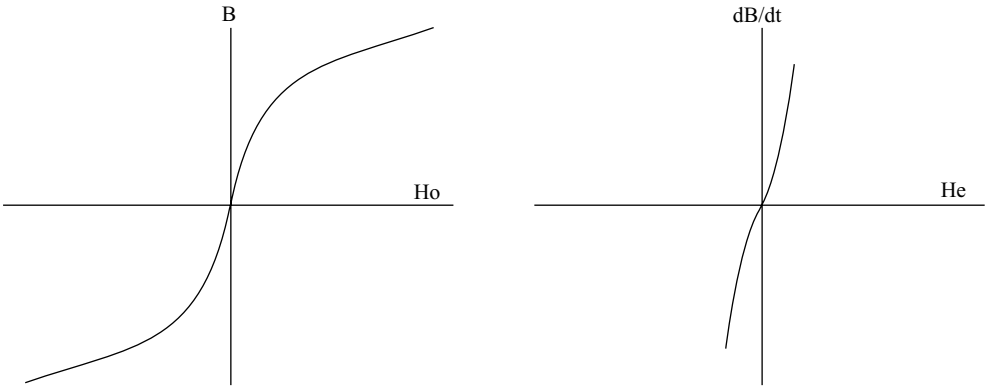

(a) (b)

Fig. 2. (a) **B** vs. $\mathbf{H}_o$ and (b) $d\mathbf{B}/dt$ vs. $\mathbf{H}_e$.

2. Modeling of ferromagnetic magnetization

2.1. Model by Fourier series

Consider the sinusoidal time t varying flux densities $\mathbf{B}$ having angular frequency ω,

$$\mathbf{B} = \mathbf{B}_m \sin(\omega t) \tag{1}$$

then, as shown in Figs 1(a) and (b), we have the distorted field intensities $\mathbf{H}$ in Eq. (2) represented in terms of Fourier series.

$$\mathbf{H} = \sum\nolimits_{a=1}^{\infty} \mathbf{H}_a \sin(a\omega t) + \sum\nolimits_{b=0}^{\infty} \mathbf{H}_b \cos(b\omega t) = \mathbf{H}_o + \mathbf{H}_e, \tag{2}$$

where $\mathbf{H}_o$ and $\mathbf{H}_e$ are the odd and even components of the distorted field $\mathbf{H}$. As shown in Figs 1(c) and (d), the odd component $\mathbf{H}_o$ and even component $\mathbf{H}_e$, are, respectively, in phase with the flux density $\mathbf{B}$ and the time derivative $d\mathbf{B}/dt$. Thereby, a combination of $\mathbf{H}_o$ with $\mathbf{B}$ yields one of the saturation curves. Also, a combination of $\mathbf{H}_e$ with $d\mathbf{B}/dt$ yields a curve which represents the hysteretic property, because $\mathbf{H}_e(d\mathbf{B}/dt)$ provides the power loss per unit volume. Figures 2(a) and (b) show the $\mathbf{B}$ vs. $\mathbf{H}_o$ and $d\mathbf{B}/dt$ vs. $\mathbf{H}_e$ curves, respectively. In the other words, by considering the relationship of Figs 2(a) and (b), it is

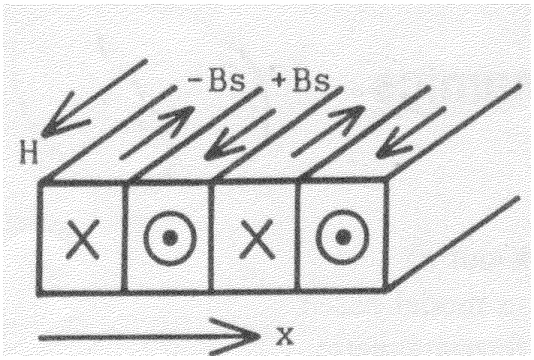

Fig. 3. Bar-like magnetic domains.

possible to derive a following Fourier based magnetization model Eq. (3).

$$\mathbf{H} = \mathbf{H}_0 + \mathbf{H}_e = \frac{1}{\mu}\mathbf{B} + \frac{1}{s}\frac{d\mathbf{B}}{dt} \tag{3}$$

where μ and s are the permeability and hysteresis coefficient, respectively [1].

2.2. Domain-based model

To derive a constitutive equation representing magnetization characteristics of ferromagnetic materials, let us consider a simple bar-like domain wall model shown in Fig. 3. When an external magnetic field $\mathbf{H}_s$ is applied, Eq. (4) can be established.

$$\mathbf{B} = \mu_0\mathbf{H}_s + n\mathbf{B}_s = \mu_0(1 + \mathbf{H}_s^{-1}\mathbf{B}_s)\mathbf{H}_s = \mu\mathbf{H}_s \tag{4}$$

Where $\mathbf{B}_s$, n, μ_0 and μ are the saturation flux density in each of the domains, number of domains in accordance with the direction of $\mathbf{H}_s$, permeability of air, and permeability of the specimen, respectively. The constitutive equation should exhibit various magnetization characteristics, such as a hysteretic property. This means that the constitutive equation must be composed of parameters not affected by past histories. One of the unique properties independent of the past histories is an ideal or anhysteretic magnetization curve. If Eq. (4) has been established for the ideal magnetization curve, then obviously Eq. (4) represents a static magnetization characteristic corresponding to each of the domain situations. This means that the permeability μ in Eq. (4) can be obtained from the ideal magnetization curve.

Differentiation of Eq. (4) with time t yields a following relation:

$$\frac{d\mathbf{B}}{dt} = \mu_0\frac{d\mathbf{H}}{dt} + \mathbf{B}_s\frac{dn}{dt} = \left(\mu_0 + \mathbf{B}_s\frac{\partial n}{\partial \mathbf{H}}\right)\frac{d\mathbf{H}}{dt} + \mathbf{B}_s\frac{\partial n}{\partial x}\frac{dx}{dt} = \mu_r\frac{d\mathbf{H}}{dt} + \mathbf{B}_s\frac{\partial n}{\partial x}v \tag{5}$$

where $\mathbf{H}$, v, and μ_r are the applied field, velocity (dx/dt) of domain movement, and reversible permeability, respectively. Consideration of Eq. (5) suggests that the induced voltage per unit area ($d\mathbf{B}/dt$) is composed of the transformer and velocity induced voltages. When a hysteresis coefficient $s(\Omega/\mathrm{m})$ is introduced into Eq. (5), the magnetic field $\mathbf{H}_d$ due to the domain movement is given by Eq. (6)

$$\mathbf{H}_d = \frac{1}{s}\mathbf{B}_s\frac{\partial n}{\partial x}v = \frac{1}{s}\left(\frac{d\mathbf{B}}{dt} - \mu_r\frac{d\mathbf{H}}{dt}\right) \tag{6}$$

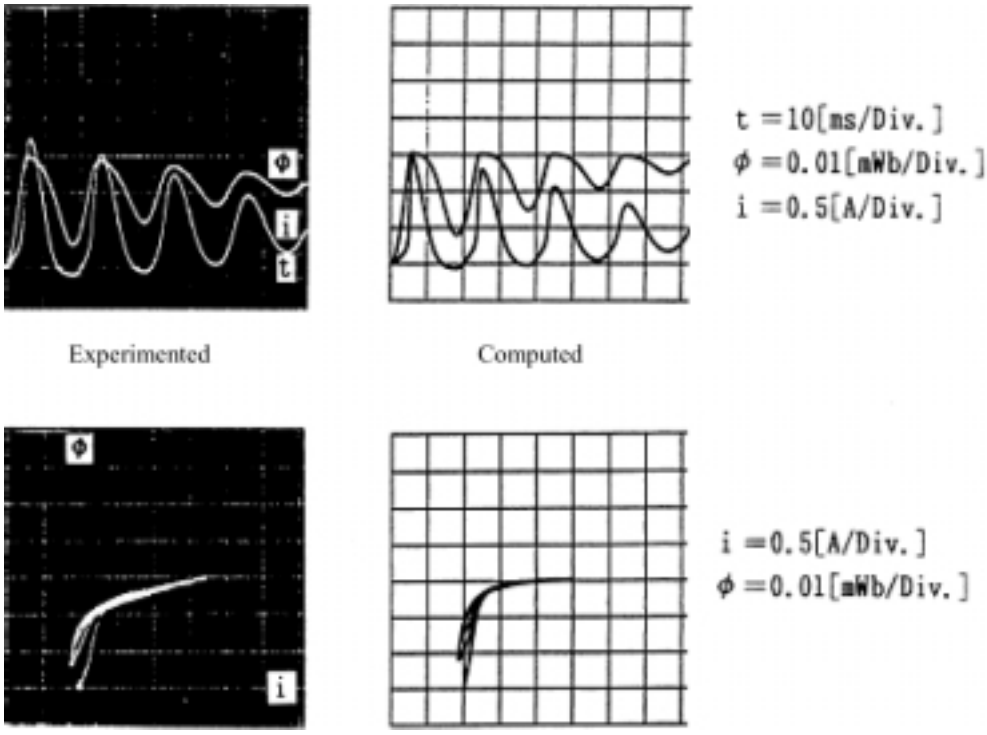

Fig. 4. Experimented and computed results (K6A, TDK).

where it has been assumed that the width of the domains is fixed and only their number changes as the specimen magnetized. Summation of the static field $\mathbf{H}_s$ in Eq. (4) and dynamic field $\mathbf{H}_d$ in Eq. (6) gives the domain-based magnetization model as [2]

$$\mathbf{H} = \mathbf{H}_s + \mathbf{H}_d = \frac{1}{\mu}\mathbf{B} + \frac{1}{s}\mathbf{B}_s\frac{\partial n}{\partial x}v = \frac{1}{\mu}\mathbf{B} + \frac{1}{s}\left(\frac{d\mathbf{B}}{dt} - \mu_r\frac{d\mathbf{H}}{dt}\right) \tag{7}$$

We had carried out intensive experimental verification of Eq. (7). Figure 4 shows one of the examples.

2.3. Preisach and composite models

According to Ref. [3], a reversing $\mathbf{H}_n$ and applied $\mathbf{H}_p$ field points are defined as shown in Fig. 5. By considering the trajectories in Fig. 5, it is obvious that **B**–**H** trajectory takes different paths depending on the reversing field $\mathbf{H}_n$. Thereby, the flux density $\mathbf{B}$ is represented as a function of applied field $\mathbf{H}_p$ as well as reversing field $\mathbf{H}_n$:

$$\mathbf{B} = f(\mathbf{H}_p, \mathbf{H}_n) \tag{8}$$

Moreover, consideration of a saturation flux density suggests that the **B**–**H** trajectories take different paths depending on the reversing fields $\mathbf{H}_n$, but always coincide at the saturation flux density. Thereby, rate of change $\partial\mathbf{B}/\partial\mathbf{H}_p$ with reversing field $\mathbf{H}_n$ takes non-zero value within the unsaturated region. This leads to the definition of the Preisach function Ψ as

$$\Psi = \frac{\partial^2\mathbf{B}}{\partial\mathbf{H}_n\partial\mathbf{H}_p} \tag{9}$$

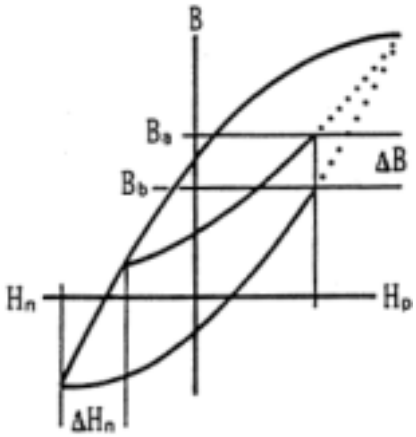

Fig. 5. Derivation of preisach model.

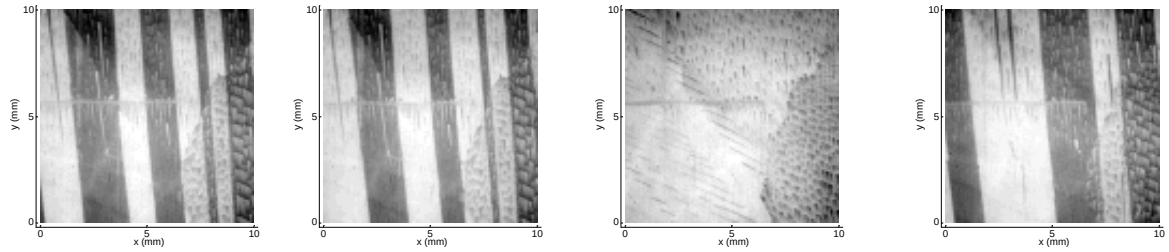

(a)*H*=0.0A/m, *B*=0.0 T (b)*H*=2.9 A/m, *B*=0.1 T (c) *H*=236.3 A/m, *B*=1.9 T (d) *H*=0.0 A/m, *B*=1.73 T

Fig. 6. Magnetic domain SEM images of the ORIENTCORE HI-B produced by Nippon Steel Co. (100 × 100 pixels, 0.1 mm/pixel).

Application of Eq. (5) to the magnetizing states shown in Fig. 5 gives

$$\mathbf{H}_p = \frac{1}{\mu}\mathbf{B}_a + \frac{1}{s}\left(\frac{\partial \mathbf{B}_a}{\partial t} - \mu_r \frac{\partial \mathbf{H}_p}{\partial t}\right) \tag{10}$$

$$\mathbf{H}_p = \frac{1}{\mu}\mathbf{B}_b + \frac{1}{s}\left(\frac{\partial \mathbf{B}_b}{\partial t} - \mu_r \frac{\partial \mathbf{H}_p}{\partial t}\right) \tag{11}$$

where the field $\Delta\mathbf{H}_m$ in Fig. 5 is so small that the parameters μ, μ_r, and s are assumed to be constants. Subtracting Eq. (10) from Eq. (11) yields

$$\frac{\Delta \mathbf{B}}{\mu} = \frac{\mathbf{B}_a - \mathbf{B}_b}{\mu} = \frac{1}{s}\left(\frac{\partial \mathbf{B}_a}{\partial t} - \frac{\partial \mathbf{B}_b}{\partial t}\right) = \frac{1}{s}\left(\frac{\partial \mathbf{B}_a}{\partial \mathbf{H}_p} - \frac{\partial \mathbf{B}_b}{\partial \mathbf{H}_p}\right)\frac{\partial \mathbf{H}_p}{\partial t} \tag{12}$$

Rearrangement of Eq. (12) gives

$$\frac{s}{\partial \mathbf{H}_p / \partial t} = \frac{\mu}{\Delta \mathbf{B}}\left(\frac{\partial \mathbf{B}_b}{\partial \mathbf{H}_p} - \frac{\partial \mathbf{B}_a}{\partial \mathbf{H}_p}\right) \tag{13}$$

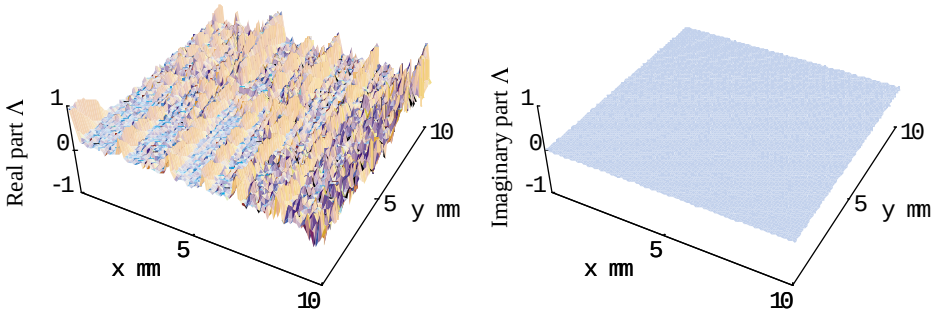

(a) $0.0 \leq H < 2.9$ A/m

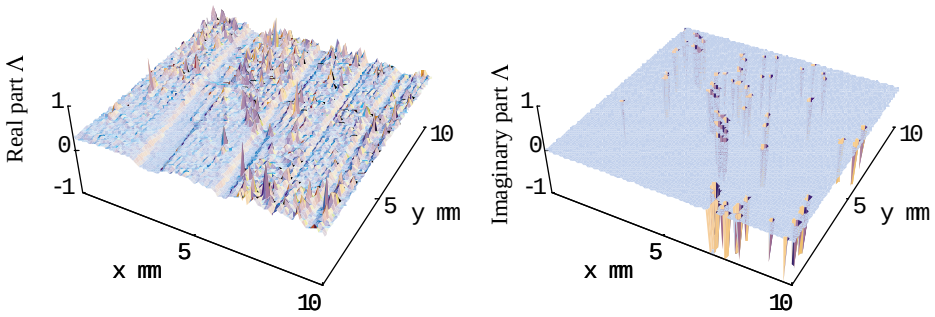

(b) $2.9 \leq H < 9.3$ A/m

Fig. 7. State transition matrices.

In Fig. 5, if the limit of $\Delta\mathbf{H}_n$ goes to zero, then $\Delta\mathbf{B}/\mu$ is simultaneously to be zero. Thus, an assumption $\Delta\mathbf{H}_n = \Delta\mathbf{B}/\mu$ leads to

$$\mathrm{Lim}_{\Delta\mathbf{H}_n \to 0} \frac{\mu}{\Delta\mathbf{B}} \left(\frac{\partial \mathbf{B}_b}{\partial \mathbf{H}_p} - \frac{\partial \mathbf{B}_a}{\partial \mathbf{H}_p} \right) = \frac{\partial^2 \mathbf{B}}{\partial \mathbf{H}_n \partial \mathbf{H}_p} \tag{14}$$

From Eqs (9), (13) and (14), the hysteresis coefficient s in Eq. (6) is related to the Preisach function Ψ by Eq. (15)

$$s = \Psi \frac{\partial \mathbf{H}}{\partial t} \tag{15}$$

Substituting Eq. (15) into Eq. (6) after some modification yields a following composite model:

$$\mathbf{H} + \frac{\mu_r}{\Psi} = \frac{1}{\mu}\mathbf{B} + \frac{1}{\Psi}\frac{d\mathbf{B}}{d\mathbf{H}} \tag{16}$$

Let us consider that the parameters μ, μ_r, and Ψ take the constants in the weakly magnetized region known as the Rayleigh region, then Eq. (16) gives

$$\mathbf{B} = \mu(\mathbf{H}_n + \mathbf{H}_p) + \frac{\mu^2}{\Psi}\left(1 - \frac{\mu_r}{\mu}\right)\left(\varepsilon^{-\frac{\mu}{\Psi}(\mathbf{H}_n + \mathbf{H}_p)} - 1\right) - \mathbf{B}_n \varepsilon^{-\frac{\mu}{\Psi}(\mathbf{H}_n + \mathbf{H}_p)} \tag{17}$$

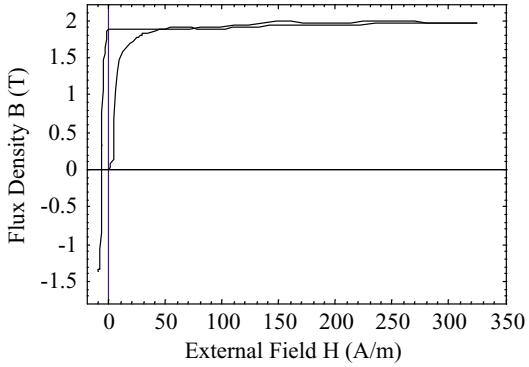

(a) Good crystallized part

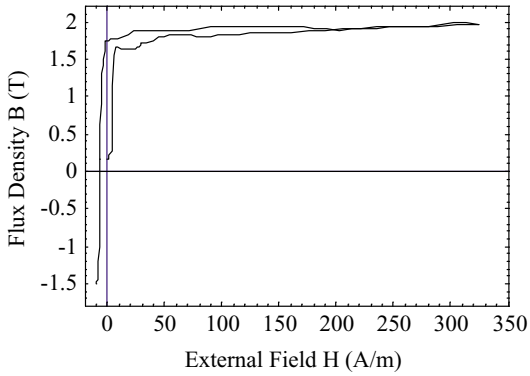

(b) Lancet part

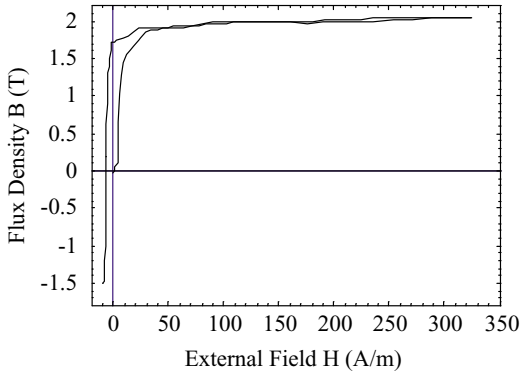

(c) Strained part

Fig. 8. Magnetization characteristics reproduced by Eq. (25).

where $\mathbf{H}_p$, $\mathbf{H}_n$ and $\mathbf{B}_n$ are the applied and reversing point fields and reversing point flux density, respectively. The fields $\mathbf{H}_p$ and $\mathbf{H}_n$ are so small that the following approximations could be held:

$$\varepsilon^{-\frac{\mu}{\Psi}(\mathbf{H}_p+\mathbf{H}_n)} \approx 1 - \frac{\mu}{\Psi}(\mathbf{H}_p + \mathbf{H}_n) + \frac{1}{2}\left[\frac{\mu}{\Psi}(\mathbf{H}_p + \mathbf{H}_n)\right]^2 \tag{18}$$

Substituting Eq. (18) into Eq. (17) and setting $\mathbf{H}_n = \mathbf{B}_n = 0$ yields

$$\mathbf{B} = \mu_r \mathbf{H}_p + \frac{1}{2}\Psi \mathbf{H}_p^2 \left(1 - \frac{\mu_r}{\mu}\right) \approx \mu_r \mathbf{H}_p + \frac{1}{2}\Psi \mathbf{H}_p^2 \tag{19}$$

where $\mu \gg \mu_r$ has been assumed. Equation (19) is obviously Rayleigh's initial magnetization curve [4]. Hence, it is revealed that the Preisach function Ψ corresponds to Rayleigh's constant. Consideration of symmetrical **B**–**H** loop condition yields the reversing flux density $\mathbf{B}_n$ as

$$\mathbf{B}_n = \mu \mathbf{H}_n + \left(\mu \mathbf{H}_n - \frac{\mu^2}{\Psi} + \frac{\mu_r \mu}{\Psi}\right) \tanh\left(\frac{\Psi}{\mu}\mathbf{H}_n\right). \tag{20}$$

After employing the approximations as these of the derivation Eq. (19), substituting this into Eq. (17) yield a lower branch of Rayleigh loop:

$$\mathbf{B} = (\mu_r + \Psi \mathbf{H}_n)\mathbf{H}_p + \frac{1}{2}(\mathbf{H}_p^2 - \mathbf{H}_n^2) \tag{21}$$

Thus, the composite model Eq. (16) is capable of deriving Rayleigh's law.

2.4. IT based model

Denoting coercive field $\mathbf{H}_c = \mu_r/\Psi$, Eq. (16) can be rewritten by

$$\mathbf{H} = \mathbf{H}_e + \mathbf{H}_c = \frac{1}{\mu}\mathbf{B} + \frac{1}{\Psi}\frac{d\mathbf{B}}{d\mathbf{H}} \tag{22}$$

so that an analytical solution of Eq. (22) assuming the constant μ and Ψ is given by

$$\mathbf{B} = \mu \mathbf{H} + [\mathbf{B}_0 - \mu \mathbf{H}]\varepsilon^{-\frac{\Psi}{\mu}\mathbf{H}} = \mathbf{B}_f + [\mathbf{B}_0 - \mathbf{B}_f]\varepsilon^{-\frac{\Psi}{\mu}\mathbf{H}} \tag{23}$$

where $\mathbf{B}_f$ and $\mathbf{B}_0$ are the final and initial flux densities, respectively.

Let us consider a characteristic value:

$$\lambda = \frac{\Psi}{\mu} \quad [\mathrm{m/A}] \tag{24}$$

then the small and large characteristic values λ correspond to the low and high field regions, respectively. Namely, the small and large λ values reveal the unsaturated and saturated states of the specimen, respectively.

When we have the three magnetic fluxes $\mathbf{B}_i$,$\mathbf{B}_{i+1}$, and $\mathbf{B}_{i+2}$ as the contrast of SEM images during the field change $\Delta\mathbf{H}$, Eq. (23) can be rewritten by

$$\mathbf{B}_{i+1} = \mathbf{B}_{i+2} + (\mathbf{B}_i + \mathbf{B}_{i+2})\varepsilon^{-\lambda\Delta\mathbf{H}} \tag{25}$$

By means of Eq. (25), the characteristic value is represented in terms of the SEM images as

$$\lambda = -\frac{1}{\Delta\mathbf{H}} \ln\left[(\mathbf{B}_{i+1} - \mathbf{B}_{i+2})^{-1}(\mathbf{B}_i - \mathbf{B}_{i+2})\right] \tag{26}$$

Figure 6 shows the domain images of a grain-oriented electrical steel sheet under the distinct magnetized states. The electrical steel sheet is the ORIENTCORE·HI-B produced by Nippon Steel Corporation and

its thickness is 0.23 mm. The backscattered electron observation was carried out using SEM accelerated to 160 kV. Changing the given domain images sequentially by the field excitation, it is easy to visualize magnetizing domain state. Figure 7 shows the characteristic value distributions determined by Eq. (26). Figure 7(a) suggests the reversible magnetic boundary displacement without pinning on the boundary. The real part shown in Figure 7(b) means the irreversible domain movement. On the other side, the imaginary part shown in Fig. 7(b) can be observed the delay of magnetic boundary displacement at the grain boundary.

Figure 8 shows the magnetization characteristics curves for which have been reproduced after increasing 111 frames from original 24 frame images by Eq. (25) [4].

Thus, by means of IT based model, we have succeeded in obtaining the magnetization characteristics in each of the image pixels on the ferromagnetic materials. This means that the magnetization characteristics can be obtained from the visualized domain images. The accuracy of this method is basically proportional to number of original SEM images. In order to enhance the accuracy, number of frames or short sampling widths should be required.

3. Conclusions

As shown above, we have derived the magnetization model by means of Fourier series. Assuming the bar-like domain walls has lead to a domain-based model. Further, a composite model by combining the Preisach with domain-based models has been derived. Analytical solution of this composite model leads to Rayleigh's law. Finally, we have proposed the IT based magnetization model, which is derived from SEM images of the ferromagnetic materials. To demonstrate the capability of this IT based model, we have drawn the magnetization characteristics at the normal, lancet and strained magnetic domains on the SEM image.

References

[1] Y. Saito, S. Hayano, H. Nakamura, Y. Kishino and N. Tsuya, A Representation of Magnetic Hysteresis by Fourier Series, *Journal of Magnetic Materials* **54–57** (1986), 1613–1614.

[2] S. Hayano, M. Namiki and Y. Saito, A Magnetization Model for Computational Magneto-dynamics, *J. Appl. Phys.*, **69**(8) (15 April, 1991), 4641–4616.

[3] Y. Saito, K. Fukushima, S. Hayano and N. Tsuya, Application of a Chua type Model to the Loss and Skin Effect Calculations, *IEEE Trans. Magn.*, **MAG-23**(5) (September, 1987), 2227–2229.

[4] H. Endo, S. Hayano, Y. Saito and T. L. Kunii, A Method of Image Processing and Its Application to Magnetodynamic Fields, *Trans. IEE of J* **120-A** (2000), 913–918, in Japanese.